PROCEEDINGS OF SCIENCE

The generalized polarizabilities of the proton

N. Sparveris[a,*]

[a] *Temple University, Department of Physics, Philadelphia, PA 19122, USA*

E-mail: sparveri@temple.edu

A fundamental property of the proton involves the system's response to an external electromagnetic (EM) field. It is characterized by the EM polarizabilities that describe how easily the charge and magnetization distributions inside the system are distorted by the EM field, such as during the Compton scattering with a real photon. When the polarizabilities are generalized to finite momentum transfer by replacing the incoming real photon of the Compton scattering process with a space-like virtual photon, they map out the deformation of the quark densities in a proton subject to an EM field. They shed light to the underlying system dynamics and provide a key for decoding the proton structure in terms of the theory of the strong interaction that binds quarks and gluons together. Recent experimental measurements at Jefferson Lab have provided high precision data, that offer guidance and present significant challenges to nuclear theory. Future experiments aim to improve further the study of the generalized polarizabilities, both in terms of the kinematic range as well as on the level of the experimental precision.

25th International Spin Physics Symposium (SPIN 2023)
September 24-29, 2023
Durham, NC, USA

*Speaker

PoS(SPIN2023)173

1. Introduction

Explaining how the proton emerges from the interactions of its quark and gluon constituents is a central goal of modern nuclear physics. The dynamics of quarks and gluons is governed by quantum chromodynamics (QCD), the theory of the strong interaction. The application of perturbation methods renders QCD calculable at large energies and momenta and offers a reasonable understanding of the nucleon structure at that scale. Nevertheless, in order to explain the emergence of nucleon's fundamental properties from the interactions of its constituents, the dynamics of the system have to be understood at long distances, where the QCD coupling constant α_s becomes large and the application of perturbative QCD is not possible. Here, theoretical calculations can rely on lattice QCD [1], a space-time discretization of the theory based on the fundamental quark and gluon degrees of freedom, starting from the original QCD Lagrangian. Another path is offered by effective field theories (EFTs), such as the chiral effective field theory [2–4], which employ hadronic degrees of freedom and is based on the approximate and spontaneously broken chiral symmetry of QCD. While steady progress has been made in recent years, we have yet to achieve a complete understanding of how the nucleon properties emerge from the underlying dynamics of the strong interaction. In order to accomplish this, the theoretical calculations require experimental guidance and confrontation with precise measurements of the system's fundamental properties.

The polarizabilities [5] are fundamental structure constants for any composite system, like the proton. The two scalar polarizabilities - the electric, α_E, and the magnetic, β_M - can be interpreted as the response of the proton's structure to the application of an external electric or magnetic field, respectively. They describe how easily the charge and magnetization distributions inside the proton are distorted by the EM field and provide the net result on the system's spatial distributions. In order to measure the polarizabilities, one must generate an electric ($\vec{E}$) and a magnetic ($\vec{H}$) field. In the case of the proton, this is provided by the photons in the Compton scattering process. The two scalar polarizabilities appear as second order terms in the expansion of the real Compton Scattering (RCS) amplitude in the energy of the photon

$$H^{(2)}_{eff} = -4\pi(\frac{1}{2}\alpha_E\vec{E}^2 + \frac{1}{2}\beta_M\vec{H}^2). \quad (1)$$

A simplistic description of the polarizabilities can be provided through the resulting effect of an electromagnetic perturbation applied to the nucleon constituents. An electric field moves positive and negative charges inside the proton in opposite directions. The induced electric dipole moment is proportional to the electric field, and the proportionality coefficient is the electric polarizability which quantifies the stiffness of the proton. On the other hand, a magnetic field has a different effect on the quarks and on the pion cloud within the nucleon, giving rise to two different contributions in the magnetic polarizability, a paramagnetic and a diamagnetic contribution, respectively. Compared to the atomic polarizabilities, which are of the size of the atomic volume, the proton electric polarizability α_E is much smaller than the volume scale of a nucleon [5]. The small magnitude underlines the stiffness of the proton, a direct consequence of the strong binding of its constituents, and indicates the intrinsic relativistic character of the system. The generalization [6] of the two scalar polarizabilities in four-momentum transfer space, $\alpha_E(Q^2)$ and $\beta_M(Q^2)$, is an extension of the static electric and magnetic polarizabilities obtained in RCS. The Generalized Polarizabilities (GP) are studied through measurements of the virtual Compton scattering (VCS) process [6] γ^*p$\rightarrow$ pγ.

The VCS is accessed experimentally through the ep→epγ reaction, where the incident real photon of the RCS process is replaced by a virtual photon. The virtuality of the incident photon (Q^2) sets the scale of the observation and allows one to map out the spatial distribution of the polarization densities in the proton, while the outgoing real photon provides the EM perturbation to the system. The meaning of the GPs is analogous to that of the nucleon form factors. Their Fourier transform will map out the spatial distribution density of the polarization induced by an EM field. They probe the quark substructure of the nucleon, offering unique insight to the underlying nucleon dynamics, and they frequently enter as input parameters in various scientific problems e.g. in the hadronic two-photon exchange corrections, which are needed for a precise extraction of the proton charge radius from muonic Hydrogen spectroscopy measurements [7].

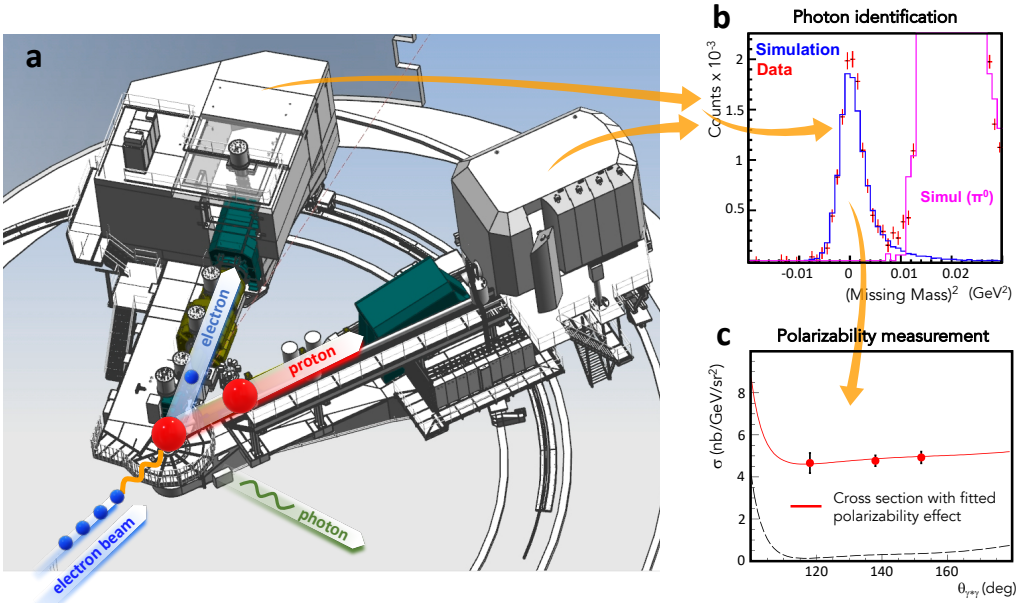

Figure 1: The VCS-I experiment at JLab
a) The experimental setup during the VCS-I experiment at Jefferson Lab. An electron beam impinges on a liquid hydrogen (red sphere) target. The interaction is mediated through the exchange of a virtual photon (orange wavy line). The scattered electron and recoil proton are detected with two magnetic spectrometers, in coincidence. The real photon (green wavy line) that is produced in the reaction provides the electromagnetic perturbation and allows to measure the proton polarizabilities. **b)** The (undetected) real photon is identified through the reconstruction of the reaction's missing mass spectrum and allows the selection of the VCS events. **c)** The cross section of the VCS reaction measures the proton generalized polarizabilities. The dashed line denotes the Bethe Heitler+Born contributions to the cross section.

2. Experimental measurements of the generalized polarizabilities

A series of early VCS experiments [8, 9, 12, 13, 32, 33] that were conducted nearly two decades ago at MAMI, JLab and Bates, shaped a first understanding of the proton electric and magnetic GPs. These measurements contradicted the naive Ansatz of a single-dipole fall-off for $\alpha_E(Q^2)$, pointing out to an enhancement at low Q^2, evidenced by two independent MAMI experiments [8, 9]. The magnetic generalized polarizability measurements were characterized by large uncertainties,

highlighting the challenges in extracting the small magnetic polarizability signal. The precision of the measurements was significantly improved a few years later during the follow-up MAMI experiment [10, 11, 34], that utilized the high resolution spectrometers setup in A1 experimental hall and explored the region Q^2=0.10 GeV^2 to 0.45 GeV^2.

The most recent measurements involve the VCS-I experiment [14] at the Thomas Jefferson National Accelerator Facility. The experiment focused on the region Q^2=0.28 GeV^2 to 0.40 GeV^2, with a special interest in the puzzling measurements of $\alpha_E(Q^2)$ that were reported at Q^2=0.33 GeV^2 [8, 9]. The experiment capitalized on the unique capabilities of the experimental setup in Hall C at Jefferson Lab that allow to conduct measurements of the scalar GPs with an unprecedented precision. Furthermore, cross section measurements were conducted for azimuthally symmetric kinematics in the photon angle, namely for $(\phi_{\gamma^*\gamma}, \pi - \phi_{\gamma^*\gamma})$. The measurement of the azimuthal asymmetry in the cross section enhances further the sensitivity in the extraction of the polarizabilities, and suppresses part of the systematic uncertainties. Moreover, the ep$\rightarrow$epπ^0 reaction was measured, simultaneously with the ep$\rightarrow$epγ reaction. This process is well understood in this kinematic regime, and its measurement offers a stringent, real-time normalization control to the measurement of the ep$\rightarrow$epγ cross section. Overall, a significant improvement was accomplished in the precision of the extracted generalized polarizabilities compared to previous measurements.

The data were acquired in Hall C of Jefferson Lab. Electrons with energies of 4.56 GeV at a beam current up to 20 μA were produced by Jefferson Lab's Continuous Electron Beam Accelerator Facility (CEBAF) and were scattered from a 10 cm long liquid-hydrogen target. The Super High Momentum Spectrometer (SHMS) and the High Momentum Spectrometer (HMS) of Hall C were used to detect in coincidence the scattered electrons and recoil protons, respectively (see Fig. 1). Both spectrometers are equipped with similar detector packages, including a set of scintillator planes that were used to form the trigger and to provide time-of-flight information and a pair of drift chambers used for tracking. The coincidence time was determined as the difference in the time-of-flight between the two spectrometers, accounting for path-length variation corrections from the central trajectory and for the individual start-times. The experimental setup offered a $\sim$1 ns (FWHM) resolution in the coincidence timing spectrum. Random coincidences were subtracted using the side (accidental) bands of the coincidence time spectrum. The events of the exclusive reaction ep$\rightarrow$epγ were identified from the missing-mass reconstruction, through a selection cut around the photon peak in the missing-mass-squared spectrum. Data were taken with an empty target in order to account for the background contributions from the target walls. Elastic scattering measurements with a proton target were performed throughout the experiment for calibration and normalization studies. The measurement of the absolute VCS cross section, $\sigma \equiv d^5\sigma/dE'_e d\Omega'_e d\Omega_{cm}$, requires the determination of the five-fold solid angle, where dE'_e, $d\Omega'_e$ is the differential energy and solid angle of the scattered electron in the laboratory frame and $d\Omega_{cm}$ is the differential solid angle of the photon in the center-of-mass frame. The experimental acceptance is calculated with the Hall C Monte Carlo simulation program, SIMC, which integrates the beam configuration, target geometry, spectrometer acceptances, resolution effects, energy losses and radiative corrections.

The cross section of the $ep \rightarrow ep\gamma$ process observes the photon that is emitted by either the lepton, known as the Bethe-Heitler (BH) process, or by the proton, the fully virtual Compton scattering (FVCS) process. The FVCS amplitude can in-turn be decomposed into a Born contribution, with the intermediate state being the nucleon, and a non-Born contribution that carries the physics

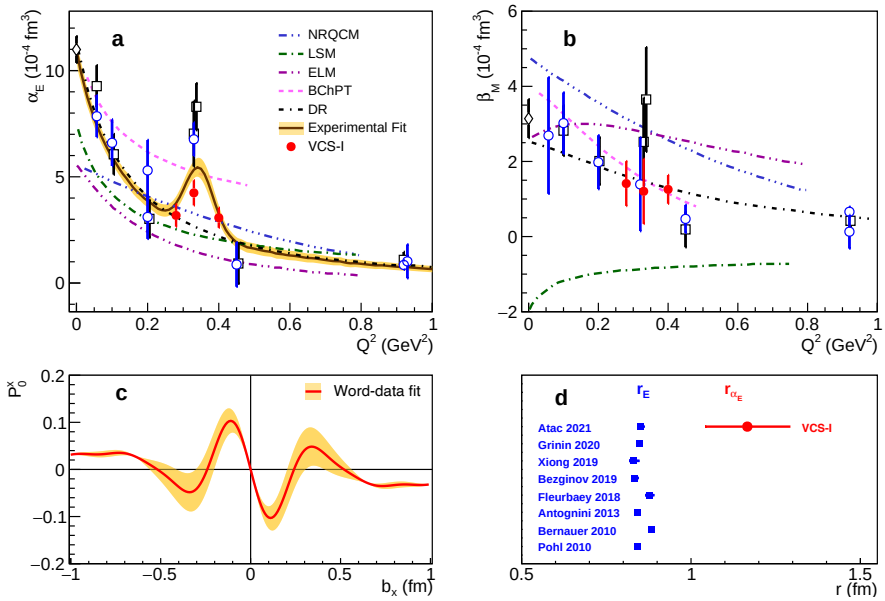

Figure 2: The generalized polarizabilities of the proton
a) The electric generalized polarizability measured in VCS-I (red circles). The world data [8–13, 31–34] (open-symbols) are shown for results that involve the Dispersion-Relations (circle) and Low-Energy-Expansion analysis (box). The theoretical calculations of BChPT [18], NRQCM [29], LSM [24], ELM [26] and DR [15–17] are also shown. **b)** The magnetic generalized polarizability. The definition of symbols and curves are the same as in (a). **c)** Induced polarization in the proton when submitted to an EM field as a function of the transverse position with photon polarization along the x axis for $b_y = 0$. The x-y defines the transverse plane, with the z axis being the direction of the fast moving protons. **d)** The proton electric polarizability radius $r_{\alpha_E} \equiv \sqrt{\langle r^2_{\alpha_E} \rangle}$ derived from the world-data. The measurements of the proton charge radius r_E [35–42] (blue points) are shown for comparison.

of interest and is parametrized by the GPs. The BH and the Born-VCS contributions are well known, calculable in terms of the proton electromagnetic form factors that are precisely measured from elastic electron scattering. The GPs were extracted from the measured cross sections through a fit that employs the dispersion relation (DR) model [15–17] for VCS. In the DR formalism, the two scalar GPs enter unconstrained and can be adjusted as free parameters, while the proton electromagnetic form factors are introduced as an input. The experimental cross sections are compared to the DR model predictions for all possible values for the two GPs, and the $\alpha_E(Q^2)$ and $\beta_M(Q^2)$ are fitted by a χ^2 minimization. The extracted electric and magnetic GPs are shown in Fig. 2. The measurements point to a local enhancement of $\alpha_E(Q^2)$ in the measured region, at the same Q^2 as previously reported in [8, 9], but with a smaller magnitude than what was originally suggested. The Q^2-dependence of the electric GP has been explored using methods that employ both traditional fits to the data using predefined functional forms, as well that are based on a data-driven technique that assumes no direct underlying functional form [14]. Both methods point to a Q^2-dependence for $\alpha_E(Q^2)$ that is consistent with the presence of a structure in the measured region, in sharp contrast with the current theoretical understanding that suggests an $\alpha_E(Q^2)$ that decreases monotonically with increasing Q^2.

The theory predictions cover a wide range of approaches such as chiral effective field theories [18–23], the linear σ-model [24, 25], the Effective Lagrangian Model [26], relativistic [27] and nonrelativistic [28, 29] constituent quark models. The $\beta_M(Q^2)$ is expected to have a smaller magnitude relative to $\alpha_E(Q^2)$. This can be explained by the competing paramagnetic and diamagnetic contributions in the proton, which largely cancel. For $\beta_M(Q^2)$, the results point to a smooth Q^2-dependence and the near-cancellation of the paramagnetic and the diamagnetic contributions in the proton at $\sim Q^2$=0.4 GeV^2. The theoretical predictions for the two generalized polarizabilities vary noticably, and the VCS-I results impose strict constraints, providing new input to the theory.

The generalized polarizabilities data allow to derive the spatial deformation of the quark distributions in the proton subject to the influence of an external electromagnetic field [30]. As shown in Fig. 2(c), we observe that the enhancement of $\alpha_E(Q^2)$ is translated to a distinct structure in the spatial distribution of the induced polarization in the proton. The distribution follows a change of sign around ~0.25 fm and exhibits a secondary maximum in the amplitude around ~0.35 fm. The GPs also allow to extract the electromagnetic polarizability radii of the proton. The mean square electric polarizability radius of the proton $\langle r^2_{\alpha_E}\rangle$ is related to the slope of the electric GP at $Q^2 = 0$ by

$$\langle r^2_{\alpha_E}\rangle = \frac{-6}{\alpha_E(0)} \cdot \frac{d}{dQ^2}\alpha_E(Q^2)\Big|_{Q^2=0}. \tag{2}$$

The slope of $\alpha_E(Q^2)$ at $Q^2 = 0$ is determined from fits to the world-data, similarly to the procedure that is followed for the extraction of the proton electric charge radius from the form factor measurements. For the mean square electric polarizability radius it is found that $\langle r^2_{\alpha_E}\rangle = 1.36 \pm 0.29\ fm^2$, a value that is considerably larger compared to the mean square charge radius of the proton, $\langle r^2_E\rangle \sim 0.7\ fm^2$ [5]. The dominant contribution to this effect is expected to arise from the deformation of the mesonic cloud in the proton under the influence of an external EM field. For the extraction of the mean square magnetic polarizability radius from the magnetic polarizability measurements, following a procedure that is equivalent to the extraction of the mean square electric

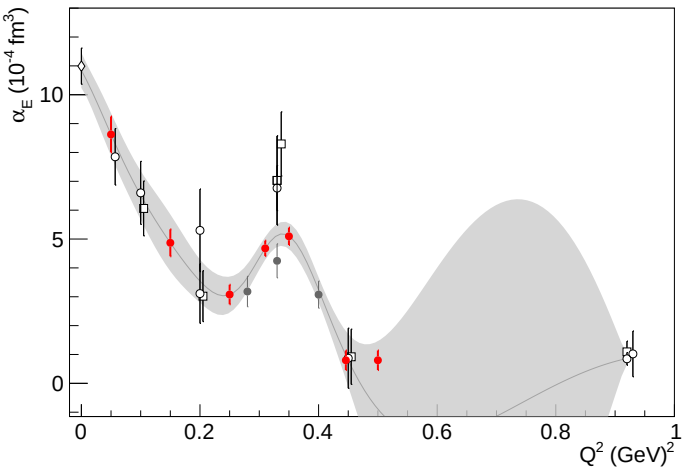

Figure 3: The VCS-II projected measurements for α_E (red circles). The world data are shown as black points (the VCS-I results are indicated with filled gray circles).

polarizability radius, one can derive $\langle r^2_{\beta_M} \rangle = 0.63 \pm 0.31\ fm^2$.

3. Future Experiments

The beamtime for the next phase of the VCS experiment at Jefferson Lab (VCS-II) has been approved by the JLab PAC51 (E12-23-001) [44]. The measurements will take place in Hall C, employing a similar experimental setup as in VCS-I, namely the SHMS and the HMS spectrometers, and will require 62 days of beam-on-target with a $E_\circ = 1.1\ GeV$ and 2.2 GeV electron beam at I=75 μA and a 10 cm liquid hydrogen target. The projected measurements of the VCS-II are shown in Fig. 3.

The recent measurements of the electric GP highlight the importance of employing alternative experimental methods for the measurement of the polarizabilities. The use of polarized and positron beams provides an alternative, powerful avenue to access the proton GPs [45]. The lepton beam charge (e) and polarization (λ) dependence of the $lp \rightarrow lp\gamma$ differential cross section is given by $d\sigma^e_\lambda = d\sigma_{\rm BH} + d\sigma_{\rm VCS} + \lambda\, d\tilde{\sigma}_{\rm VCS} + e\,(d\sigma_{\rm INT} + \lambda\, d\tilde{\sigma}_{\rm INT})$, where $d\sigma$ ($d\tilde{\sigma}$) are the polarization independent (dependent) contributions which are even (odd) functions of the azimuthal angle ϕ. The $d\sigma_{\rm INT}$ involves the real part of the VCS amplitude that contains the GP effects, while $d\tilde{\sigma}_{\rm INT}$ is proportional to the imaginary part of the VCS amplitude which does not depend on the GPs. Combining lepton beams of opposite charge and different polarization enables the complete separation of the four unknown INT and VCS contributions. More specifically, using unpolarized electron and positron beams, one can construct the unpolarized beam-charge asymmetry (BCA) A^C_{UU} as

$$A^C_{UU} = \frac{(d\sigma^+_+ + d\sigma^+_-) - (d\sigma^-_+ + d\sigma^-_-)}{d\sigma^+_+ + d\sigma^+_- + d\sigma^-_+ + d\sigma^-_-} = \frac{d\sigma_{\rm INT}}{d\sigma_{\rm BH} + d\sigma_{\rm VCS}}.$$

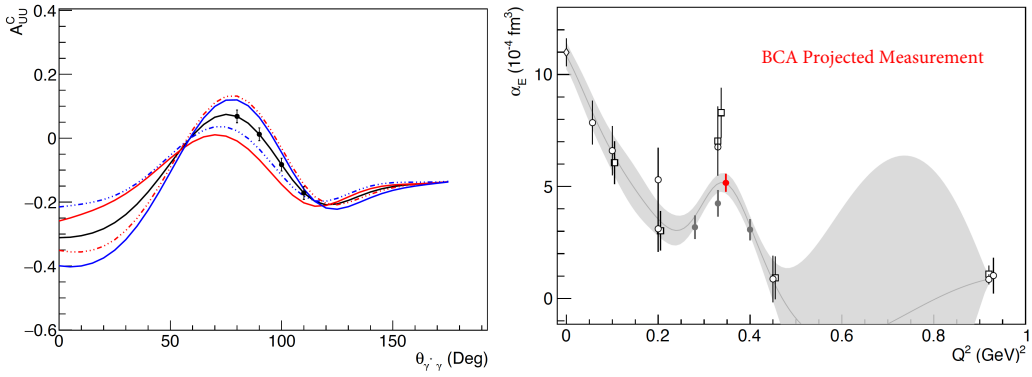

Figure 4: Beam charge asymmetry projected measurements with a positron and an electron beam. Left panel: measurements at a fixed bin at $W = 1170\ MeV$ and $\phi = 30^o$. The black curve corresponds to mass scale parameters Λ_α=Λ_β=0.7. The two red (blue) curves explore the sensitivity to the electric (magnetic) GP by varying the Λ_α (Λ_β) from 0.5 to 0.9. Right panel: the projected measurement for the α_E from the BCA measurements is shown in red, along with the world data.

With polarized lepton beams, one can further construct the lepton beam-spin asymmetry (BSA)

$$A^e_{LU} = \frac{d\sigma^e_+ - d\sigma^e_-}{d\sigma^e_+ + d\sigma^e_-} = \frac{d\tilde{\sigma}_{\rm VCS} + e d\tilde{\sigma}_{\rm INT}}{d\sigma_{\rm BH} + d\sigma_{\rm VCS} + e\, d\sigma_{\rm INT}}.$$

The theoretical groundwork and a first theoretical exploration for the potential of this type of measurements has been conducted in [45]. These studies have shown that the un-polarized BCA asymmetries and the polarized BSA asymmetries exhibit significant sensitivity to both the scalar GPs. A combination of both types of asymmetries, is powerful towards separating the contribution from the $d\tilde{\sigma}_{\rm VCS}$ and $d\tilde{\sigma}_{\rm INT}$ terms, offering both sensitivity to the GPs as well as a cross-check of the unitarity input in the dispersive formalism, as discussed in [45]. A Letter-of-Intent for the measurement of the polarizabilities using this method was submitted to the JLab PAC51 (LOI12-23+001), e.g. see Fig. 4, and the collaboration has received the recommendation to proceed with the submission of a full proposal.

References

[1] Wilson, K. G. Confinement of quarks. *Phys. Rev. D* **10**, 2445 (1974).

[2] Weinberg, S. Nuclear forces from chiral lagrangians. *Phys. Lett. B* **251**, 288 (1990).

[3] Weinberg, S. Effective chiral lagrangians for nucleon-pion interactions and nuclear forces. *Nucl. Phys. B* **363**, 3 (1991).

[4] Weinberg, S. Three-body interactions among nucleons and pions. *Phys. Lett. B* **295**, 114 (1992).

[5] Zyla, P. A. *et al.* Review of Particle Physics. *Prog. Theor. Exp. Phys.* **2020**, 083C01 (2020).

[6] Fonvieille, H., Pasquini, B. and Sparveris, N. Virtual Compton Scattering and Nucleon Generalized Polarizabilities. *Prog. Part. Nucl. Phys.* **113**, 103754 (2020).

[7] Pasquini, B. and Vanderhaeghen, M. Dispersion Theory in Electromagnetic Interactions. *Annu. Rev. Nucl. Part. Sci.* **68**, 75-103 (2018).

[8] Roche, J. *et al.* First Determination of Generalized Polarizabilities of the Proton by a Virtual Compton Scattering Experiment. *Phys. Rev. Lett.* **85**, 708-711 (2000).

[9] Janssens, P. *et al.* A new measurement of the structure functions PLL-PTT/ε and PLT in virtual Compton scattering at $Q^2 = 0.33(GeV/c)^2$. *Eur. Phys. J.* **A37**, 1-8 (2008)

[10] Beričič, J. *et al.* New Insight in the Q^2 Dependence of Proton Generalized Polarizabilities. *Phys. Rev. Lett.* **123**, 192302 (2019)

[11] Fonvieille, H. *et al.* Measurement of the generalized polarizabilities of the proton at intermediate Q^2. *Phys. Rev. C* **103**, 025205 (2021)

[12] Laveissiere, G. *et al.* Measurement of the Generalized Polarizabilities of the Proton in Virtual Compton Scattering at $Q^2 = 0.92$ and 1.76 GeV^2. *Phys. Rev. Lett.* **93**, 122001 (2004)

[13] Fonvieille, H. *et al.* Virtual Compton scattering and the generalized polarizabilities of the proton at Q^2 = 0.92 and 1.76 GeV^2. *Phys. Rev. C* **86**, 015210 (2012)

[14] R. Li, et al., Nature **611**, 265 (2022)

[15] Pasquini, B., Drechsel, D.,Gorchtein, M., Metz, A., and Vanderhaeghen, M. Dispersion relation formalism for virtual Compton scattering and the generalized polarizabilities of the nucleon. *Phys. Rev. C* **62**, 052201(R) (2000).

[16] Pasquini, B., Gorchtein, M., Drechsel, D., Metz, A. and Vanderhaeghen, M. Dispersion relation formalism for virtual Compton scattering off the proton. *Eur. Phys. J. A* **11**, 185 (2001).

[17] Drechsel, D., Pasquini, B. and Vanderhaeghen, M. Dispersion relations in real and virtual Compton scattering. *Phys. Rep.* **378**, 99 (2003).

[18] Lensky, V., Pascalutsa, V. and Vanderhaeghen, M. Generalized polarizabilities of the nucleon in baryon chiral perturbation theory. *Eur. Phys. J. C* **77**, 119 (2017).

[19] Hemmert,T. R., Holstein, B., Knochlein G., Scherer S. Virtual Compton scattering off the nucleon in chiral perturbation theory. *Phys. Rev. D* **55**, 2630 (1997).

[20] Hemmert, T. R., Holstein, B., Knochlein, G., Scherer, S. Generalized polarizabilities and the chiral structure of the nucleon. *Phys. Rev. Lett.* **79**, 22 (1997).

[21] Hemmert, T. R., Holstein, B., Knochlein, G., Drechsel, D. Generalized polarizabilities of the nucleon in chiral effective theories. *Phys. Rev. D* **62**, 014013 (2000).

[22] Kao, C. W., Vanderhaeghen, M. Generalized spin polarizabilities of the nucleon in heavy baryon chiral perturbation theory at next-to-leading order. *Phys. Rev. Lett.* **89**, 272002 (2002).

[23] Kao, C. W., Pasquini, B., Vanderhaeghen, M. New predictions for generalized spin polarizabilities from heavy baryon chiral perturbation theory. *Phys. Rev. D* **92**, 119906 (2015).

[24] Metz, A., Drechsel, D. Generalized polarizabilities of the nucleon studied in the linear sigma model. *Z. Phys. A* **356**, 351 (1996).

[25] Metz, A., Drechsel, D. Generalized polarizabilities of the nucleon studied in the linear sigma model 2. *Z. Phys. A* **359**, 165 (1997).

[26] Korchin, A.and Scholten, O. Nucleon polarizabilities in virtual Compton scattering. *Phys. Rev. C* **58**, 1098 (1998)

[27] Pasquini, B. and Salme, G. Nucleon generalized polarizabilities within a relativistic constituent quark model. *Phys. Rev. C* **57**, 2589 (1998).

[28] Liu, G. Q., Thomas, A. W., Guichon, P. A. M. Virtual Compton scattering from the proton and the properties of nucleon excited states. *Aust. J. Phys.* **49**, 905 (1996).

[29] Pasquini, B., Scherer, S. and Drechsel, D. Generalized polarizabilities of the proton in a constituent quark model revisited. *Phys. Rev. C* **63**, 025205 (2001).

[30] Gorchtein, M., Lorce, C., Pasquini, B., Vanderhaeghen, M. Light-front interpretation of Proton Generalized Polarizabilities. *Phys. Rev. Lett.* **104**, 112001 (2010).

[31] Mornacchi, E. *et al.* Measurement of Compton scattering at MAMI for the extraction of the electric and magnetic polarizabilities of the proton. *arXiv:2110.15691* , (2010)

[32] Bourgeois, P. *et al.* Measurements of the generalized electric and magnetic polarizabilities of the proton at low Q^2 using the VCS reaction. *Phys. Rev. Lett.* **97**, 212001 (2006)

[33] Bourgeois, P. *et al.* Measurements of the generalized electric and magnetic polarizabilities of the proton at low Q^2 using the virtual Compton scattering reaction. *Phys. Rev. C* **84**, 035206 (2011)

[34] Blomberg, A. *et al.* Virtual Compton Scattering measurements in the nucleon resonance region. *Eur. Phys. J. A* **55**, 182 (2019).

[35] Pohl, R. *et al.* The size of the proton. *Nature* **466**, 213-216 (2010)

[36] Antognini, A. *et al.* Proton structure from the mea-surement of 2S–2P transition frequencies of muonic hydrogen. *Science* **339**, 417–420 (2013)

[37] Xiong, W. *et al.* A small proton charge radius from an electron–proton scattering experiment. *Nature* **575**, 147–150 (2019)

[38] Fleurbaey, H. *et al.* New measurement of the 1S–3S transition frequency of hydrogen: contribution to the proton charge radius puzzle. *Phys. Rev. Lett.* **120**, 182001 (2018)

[39] Bezginov, N. *et al.* A measurement of the atomic hydrogen Lamb shift and the proton charge radius. *Science* **365**, 1007 (2019)

[40] Bernauer, J. C. *et al.* High-Precision Determinatio nof the Electric and Magnetic Form Factors of the Proton. *Phys. Rev. Lett.* **105**, 242001 (2010)

[41] Atac, H. *et al.* Charge radii of the nucleon from its flavor dependent Dirac form factors. *Eur. Phys. J. A* **57**, 65 (2021)

[42] Grinin, A. *et al.* Two-photon frequency comb spectroscopy of atomic hydrogen. *Science* **370**, 1061–1066 (2020)

[43] Atac, H. *et al.* Measurement of the neutron charge radius and the role of its constituents. *Nature Commun.* **12**, 1759 (2021)

[44] H. Atac et al., arXiv:2308.07197

[45] B. Pasquini and M. Vanderhaeghen, Eur. Phys. J. A **57** (2021) 11, 316